Tissue Eng Regen Med (2019) 16(3):237–251
https://doi.org/10.1007/s13770-019-00184-0

Online ISSN 2212-5469

ORIGINAL ARTICLE

Preparation and Characterization of Nanocomposite Scaffolds (Collagen/β-TCP/SrO) for Bone Tissue Engineering

Hamid Goodarzi[1] · Sameereh Hashemi-Najafabadi[1] · Nafiseh Baheiraei[2] · Fatemeh Bagheri[3]

Received: 30 September 2018 / Revised: 27 January 2019 / Accepted: 29 January 2019 / Published online: 21 March 2019

Abstract

BACKGROUND: Nowadays, production of nanocomposite scaffolds based on natural biopolymer, bioceramic, and metal ions is a growing field of research due to the potential for bone tissue engineering applications.

METHODS: In this study, a nanocomposite scaffold for bone tissue engineering was successfully prepared using collagen (COL), beta-tricalcium phosphate (β-TCP) and strontium oxide (SrO). A composition of β-TCP (4.9 g) was prepared by doping with SrO (0.05 g). Biocompatible porous nanocomposite scaffolds were prepared by freeze-drying in different formulations [COL, COL/β-TCP (1:2 w/w), and COL/β-TCP-Sr (1:2 w/w)] to be used as a provisional matrix or scaffold for bone tissue engineering. The nanoparticles were characterized by X-ray diffraction, Fourier transforms infrared spectroscopy and energy dispersive spectroscopy. Moreover, the prepared scaffolds were characterized by physicochemical properties, such as porosity, swelling ratio, biodegradation, mechanical properties, and biomineralization.

RESULTS: All the scaffolds had a microporous structure with high porosity (~ 95–99%) and appropriate pore size (100–200 μm). COL/β-TCP-Sr scaffolds had the compressive modulus (213.44 ± 0.47 kPa) higher than that of COL/β-TCP (33.14 ± 1.77 kPa). *In vitro* cytocompatibility, cell attachment and alkaline phosphatase (ALP) activity studies performed using rat bone marrow mesenchymal stem cells. Addition of β-TCP-Sr to collagen scaffolds increased ALP activity by 1.33–1.79 and 2.92–4.57 folds after 7 and 14 days of culture, respectively.

CONCLUSION: In summary, it was found that the incorporation of Sr into the collagen-β-TCP scaffolds has a great potential for bone tissue engineering applications.

Keywords Collagen · β-TCP · SrO · Freeze drying · Bone tissue engineering

✉ Sameereh Hashemi-Najafabadi
s.hashemi@modares.ac.ir

✉ Nafiseh Baheiraei
n.baheiraei@modares.ac.ir

[1] Department of Biomedical Engineering, Faculty of Chemical Engineering, Tarbiat Modares University, Jalal ale Ahmad Highway, P.O. Box 14115-114, Tehran, Iran

[2] Tissue Engineering and Applied Cell Sciences Division, Department of Hematology, Faculty of Medical Sciences, Tarbiat Modares University, Jalal ale Ahmad Highway, P.O. Box 14115-331, Tehran, Iran

[3] Department of Biotechnology, Faculty of Chemical Engineering, Tarbiat Modares University, Jalal ale Ahmad Highway, P.O. Box 14115-114, Tehran, Iran

1 Introduction

Significant progress has been made recently in bone tissue engineering to provide higher regeneration rates with ideal mechanical properties suitable for bone tissues [1, 2]. Scaffolds are necessary to support the damaged tissues, allowing the cells to proliferate, differentiate, and gradually replaced by new bone tissue [3–5]. The scaffolds for bone tissue engineering should have appropriate biocompatibility, biodegradation rate, osteoconductive ability to promote new bone formation, with mechanical properties to ensure the compatibility with surrounding tissues, and porous structure to provide sufficient space for cell proliferation.

The scaffolds comprising synthetic or natural biopolymers and bioceramics, such as β-tri-calcium phosphate (β-TCP) and hydroxyapatite (HA) or their composites are used as biomedical materials for bone regeneration [1, 6, 7]. Collagen and β-TCP are the main organic and inorganic components of natural bone and are investigated as scaffolds for bone tissue engineering [8–11]. Collagen has unique features including appropriate osteoconductivity, bioactivity, biodegradability and excellent biocompatibility [7, 12].

Calcium phosphate ceramics have suitable osteoconductivity and biocompatibility for bone tissue engineering. β-TCP is currently one of the most frequently used calcium phosphates for bone tissue application [10, 13–16]. In addition to being biodegradable, osteoconductive and resorbable, β-TCP has a Ca/P ratio similar to that of natural bone [6, 17–20]. Several studies have reported that β-TCP, as a bioactive material, has excellent biocompatibility and moderate degradation rate compared to HA and α-TCP. β-TCP resorption rate is higher than that of crystalline hydroxyapatite with a very low resorption rate. The solubility of other calcium phosphate ceramics is also higher than bone tissue regeneration rate, making them unsuitable for the progressive process of new bone tissue replacement [6, 17–21]. Moreover, β-TCP can promote cell attachment, increase differentiation and proliferation of mesenchymal stem cells (MSCs). Previously, we prepared COL/β-TCP scaffold and the results showed that the presence of β-TCP particles embedded in the collagen matrix, could promote the differentiation of MSCs to osteoblasts with higher alkaline phosphatase (ALP) activity and mechanical strength of the scaffold compared to pure collagen scaffold. More importantly, *in vivo* subcutaneous vascularization markedly increased in COL/β-TCP compared to pure collagen [22].

Moreover, the inorganic phase of natural bone is enriched with many metallic ions, and their positive effects on bone tissue regeneration have been demonstrated elsewhere [23]. Several studies have also shown that Sr^{2+}, Zn^{2+}, Mg^{2+}, Cu^{2+} and Co^{2+} ions play a vital role in osteogenesis or angiogenesis. Among them, strontium (Sr^{2+}) has been shown to enhance bone regeneration, due to its simultaneous stimulatory effect on the osteoblast-mediated bone formation, as well as inhibitory effect on the osteoclast-mediated bone resorption [24–28]. Several attempts have been made to introduce SrO into β-TCP structure to enhance its physicochemical properties as well as biological responses of the scaffold. These improvements are due to the changes in the physicochemical properties of CaPs, such as crystallinity, solubility, surface energy, microstructure, and dissolution rate [24, 28–34]. Strontium is believed to participate in dental tissue mineralization because of its similar physicochemical properties to calcium. Since bacterial infection can prevent the process of bone regeneration, recent studies have reported that incorporation of Sr into the dental and orthopedic biomaterials, such as β-TCP and HA, may inhibit the bacterial growth [35].

As calcium phosphate containing Sr has been shown to have the potential of angiogenic stimulation during the early phase of bone repair process, it can be used to fabricate bone scaffolds. Released Sr can induce VEGF expression in the host cells, which in turn promotes angiogenesis and more bone defect repair *in vivo* [34, 36–38].

Banerjee et al. [33] prepared SrO and MgO doped with β-TCP by milling media system, and showed that both MgO and SrO can affect the physicochemical and biological properties of β-TCP. It has been shown that β-TCP–MgO/SrO scaffold has slower degradation rate than pure β-TCP scaffold during the implantation. They also showed that, the presence of Sr and Mg have beneficial effects on the cell adhesion and osteogenic differentiation of MSCs. Tarafder et al. [24] also studied the presence of strontium and magnesium in 3D printed macroporous β-TCP scaffolds on *in vivo* osteogenesis. Histomorphology analysis showed a significant increase in bone formation, and mineralization inside Sr-Mg doped β-TCP scaffolds compared with pure β-TCP scaffolds. In another study, strontium doped calcium phosphate spheres (SrCPS) was prepared by Hulsart-Billstrum et al. [32], and cell viability and cytotoxicity were evaluated with different concentrations (0–1000 μg/mL) of SrCPS. The SrCPS showed no toxicity at all concentrations. SrCPS implantation induced bone formation in comparison to pure CPS, resulting in complete resorption and defect consolidation.

In this study, we developed a novel COL/β-TCP-Sr nanocomposite scaffold using the freeze-drying method. At first, SrO was doped with β-TCP particles (β-TCP-Sr), and the synthesized β-TCP-Sr nanoparticles were then added as inorganic additives to collagen for scaffold fabrication. The aim of this study was to evaluate the effect of Sr addition on the physicochemical and biological properties of COL/β-TCP scaffold.

2 Materials and methods

2.1 Materials

β-TCP sintered powder, anhydrous ethanol, N-(3-dimethylaminopropyl)-N′-ethylcarbodiamide hydrochloride (EDC), N-hydroxysuccinimide (NHS) and SrO were purchased from Sigma Aldrich (St. Louis, MO, USA). An aqueous solution of type I collagen prepared from goat tendon (3.2 mg/mL, pH 2.9) in acetic acid (CH_3COOH)

was purchased from Nitta Gelatin Inc (Madison, NY, USA). Dulbecco's modified Eagle's medium (DMEM), trypsin–EDTA, antibiotics (penicillin/streptomycin), fetal bovine serum (FBS), phosphate buffered saline (PBS) were purchased from Gibco (Waltham, MA, USA).

2.2 Preparation of nanoparticles and nanocomposite scaffolds

β-TCP powder (4.9 g) was doped with 0.05 g SrO, by mixing in 7.5 mL anhydrous ethanol in a ball-milling system containing 100 g of 5 mm Zirconia milling media. In order to minimize the particle size and increase the homogeneity of the powder, the mixture was milled for 6 h at 70 rpm. After milling, the obtained powder (β-TCP-Sr) was dried in an oven at 60 °C for 72 h [24]. Collagen solution was mixed with β-TCP or β-TCP-Sr to obtain a homogenized solution after 6 h. The solution was poured into a cylindrical mold (5 cm in length and 1 cm in diameter) and then frozen at − 20 °C for 6 h, and stored at − 80 °C overnight. Three different types of scaffolds were prepared by freeze drying technique: collagen (COL), collagen/β-TCP (COL/β-TCP (1:2 w/w)), and collagen/β-TCP-Sr (COL/β-TCP-Sr (1:2 w/w)). The prepared scaffolds were cross-linked at room temperature, using a solution of 50 mM EDC/25 mM NHS in 10 mL of 98% V/V ethanol. The samples were then washed in deionized water to remove the unreacted EDC/NHS solution for 24 h with water change every 6 h. Finally, the samples were freeze-dried to obtain porous scaffolds. A schematic picture of the scaffolds preparation process is shown in Fig. 1.

2.3 Isolation and expansion of rat bone marrow mesenchymal stem cells (rBM-MSCs)

For cell culture studies, bone marrow (BM) was collected from the femurs of three Wistar rats aged 4-6 weeks. Briefly, the femurs and tibiae were dissected by cutting at the joints, and the bones were carefully cleaned and washed twice with PBS. The bones were held with forceps in a culture dish, and a needle was inserted into the bone cavity. The BM was flushed with DMEM and the bone cavities washed twice again. The medium containing BM was then centrifuged for 5 min at 1200 rpm. BM was mixed with the complete medium, plated in 75 cm^2 culture flasks and incubated at 37 °C and 5% CO_2, with medium change twice a week. For the present study, BM-MSCs were used after 3 passages [39, 40].

2.4 Characterization

2.4.1 Characterization of the prepared nanoparticles

Phase analysis of β-TCP and β-TCP-Sr samples was carried out by X-ray diffraction (XRD; Philips, Amsterdam, Netherlands), using Co Kα radiation without any filter. Each run was investigated with 2θ values of 10–90 at a step size of 0.02 and a count time of 0.5 s per step. The recorded XRD patterns and quantified phase composition were analyzed using X'Pert High Score Plus software. Fourier transforms infrared spectroscopy (FTIR) analysis was conducted using FTIR spectrophotometer manufactured by Perkin- Elmer (Waltham, MA, USA). Briefly, a few milligram of the sample was mixed with KBr at a ratio of 1/100, pressed into the disks, and assessed at 400 to 4000 cm^2. In order to determine the percentage of Ca, P, O and Sr in β-TCP and β-TCP-Sr particles, an energy dispersive spectroscopy (EDAX; Rontec, Mahwah, NJ, USA) analysis was carried out. The samples were placed on the aluminum supports, and air-dried at 25 °C. For dynamic light scattering (DLS) analysis, β-TCP and β-TCP-Sr were prepared in ethanol anhydrous at 0.1 mg/mL concentration. The mean hydrodynamic diameter and size distribution of β-TCP and β-TCP-Sr were measured by DLS (ZSP, Malvern Instrument, Worcestershire, UK) equipped with helium–neon laser and scattering angle [41].

2.4.2 Characterization of the nanocomposite scaffolds

FTIR was performed to investigate the interaction between COL, COL/β-TCP and COL/β-TCP-Sr in the range of 400-4000 cm^{-1} at a scan speed of 23 scans/min with a resolution of 1 cm^{-1} in KBr-diluted medium. Morphology of the prepared scaffolds was investigated by scanning electron microscopy (SEM; XL30, Philips, Amsterdam, Netherlands). The samples were also quenched in liquid nitrogen and broken into pieces for the cross-sectional study. Porosity of the prepared scaffolds was measured using Archimedes' principle. Briefly, the scaffolds were completely immersed in a container filled with ethanol until they were saturated. The porosity was then calculated according to the following Eq.:

$$\text{Porosity}\,(\%) = \frac{(w_2 - w_3 - w_s)/\rho_e}{(w_1 - w_3)/\rho_e} \times 100$$

where W_1 is the weight of the container filled with ethanol; W_2 is the weight of the container filled with ethanol including the scaffold; W_3 is the weight of the container filled with ethanol after removal of the scaffold; W_s is weight of the dry scaffold and ρ_e is ethanol density [22]. Swelling ratio was used to evaluate the swelling behavior of the scaffolds. Briefly, the scaffolds were placed in PBS

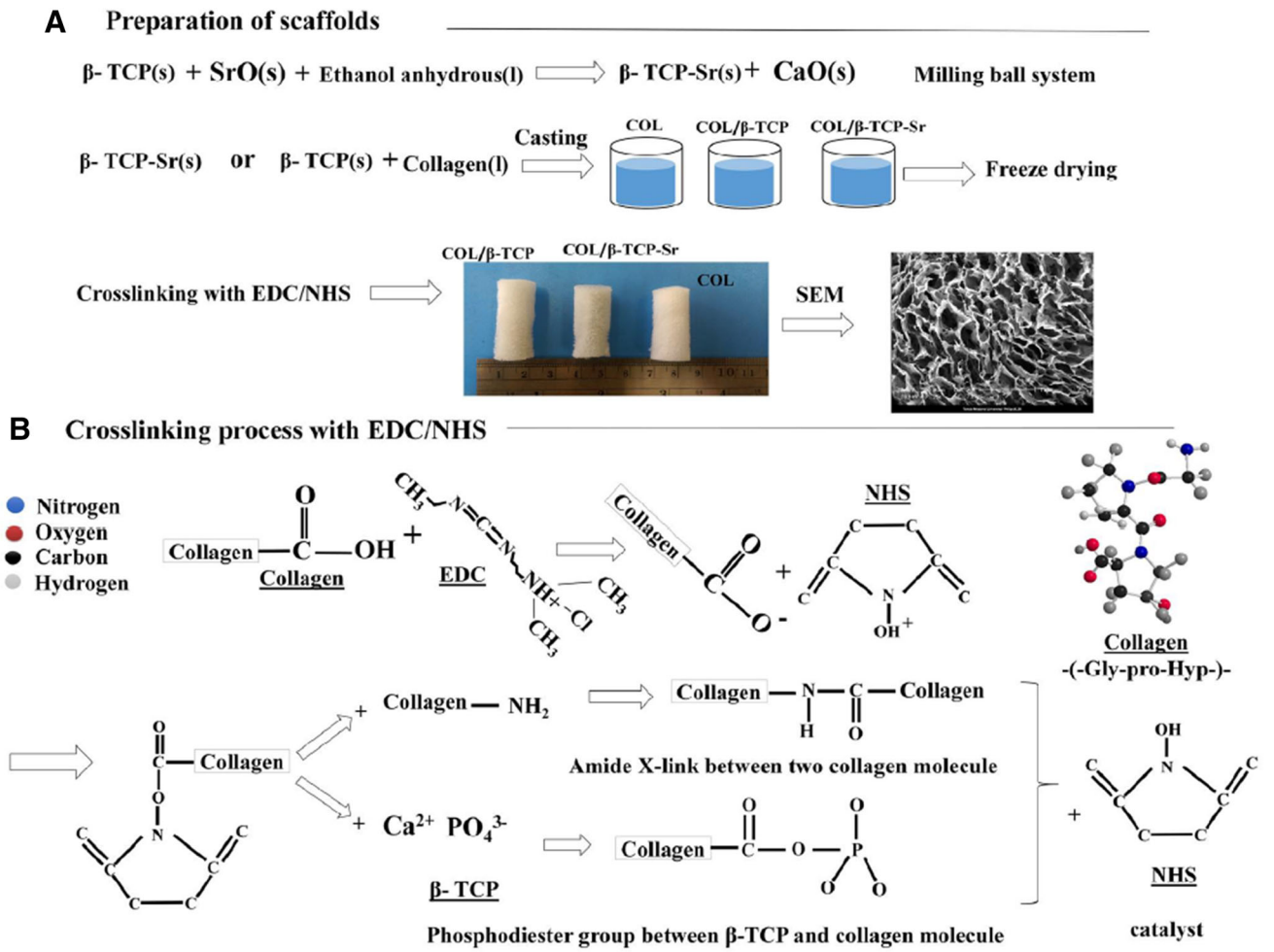

Fig. 1 **A** A schematic representation of the scaffold preparation process for COL, COL/β-TCP and COL/β-TCP-Sr. **B** The cross-linking reaction mechanism between collagen and β-TCP by EDC/NHS

(pH 7.4) solution at 37 °C in humidified atmosphere of 5% CO_2 for 1, 3, 24 and 48 h. Every time, the wet weight was recorded after taking out the scaffolds and removing the surface water by a filter paper [22]. The swelling ratio was evaluated using the following Eq.:

$$\text{Swelling ratio} = (\text{wet weight} - \text{dry weight})/\text{dry weight}$$

The prepared scaffolds were studied for their *in vitro* degradation in PBS solution, according to our previous work [22]. The scaffolds of equal weight in 10 mL PBS (pH 7.4) were incubated in a water bath at 37 °C. To prevent the fungal growth over the experimental period, sodium azide (0.1 wt%) was added to the PBS. The scaffolds were removed at predetermined time-periods (15, 30 and 60 days), washed in distilled water and dried in a vacuum desiccator. The weight loss percentage was calculated using the following Eq.:

$$\text{Weight loss}\,(\%) = (W_1 - W_2)/W_1 \times 100$$

where W_1 and W_2 are the weight of the scaffolds before and after degradation, respectively. Compression tests on the scaffolds were conducted at room temperature (25 °C) using a conventional testing machine (H10KS, Hounsfield, UK) by applying 250 N load at a loading rate of 1 mm min^{-1} until the sample was compressed to 50% of its original height. All samples were cut into cylindrical shapes (30 mm in height and 10 mm in diameter, n = 2/group). The compressive modulus was evaluated from the slope of the stress–strain curve in the elastic region. The biomineralization activity of COL/β-TCP and COL/β-TCP-Sr scaffolds was measured by immersion of each scaffold in simulated body fluid (SBF) and incubation at 37 °C and 5% CO_2 for 3 and 7 days. The scaffolds were then removed from the SBF, washed with deionized water, and dried. The morphology (crystals on the surface) and the amount of Ca and P formed on the scaffolds were evaluated using SEM and EDAX, respectively [42].

2.4.3 Cell evaluations

rBM-MSCs were seeded on the scaffolds (10×10^3 cells/scaffold) in 96-well plates. DMEM, supplemented with FBS (10% v/v) and penicilin/streptomycin (1% v/v) was used as the culture medium. Prior to cell seeding, the scaffolds were sterilized by immersion in ethanol 70%, for 15 min, then washed with PBS and treated with ultraviolet radiation for 20 min. Cytotoxicity of the scaffolds was evaluated by MTT assay. Briefly, the scaffolds were seeded in 96-well plate (n = 3). After 24, 48 and 96 h of incubation, a cytocompatibility assessment was carried out using 3-[4, 5-dimethylthiazol-2-y1]-2, 5-diphenyltetrazolium bromide (MTT, Sigma-Aldrich, St. Louis, MO, USA) colorimetric assay. The culture medium was removed, and 200 µL a solution containing a ratio of 5:1 from media and MTT (5 mg/mL in PBS) was then added to each well and incubated for 2.5 h at 37 °C and 5% CO_2. Then, the medium was removed, and the formazan precipitates were dissolved in dimethyl sulfoxide (DMSO, Sigma-Aldrich, St. Louis, MO, USA). Absorbance was measured at 545 nm using a microplate reader (Thermo Scientific, Mahwah, NJ, USA). Cellular attachment on the scaffolds was evaluated by SEM. After 48 h, the attached cells were fixed in 2.5% (v/v) glutaraldehyde for 1 h. The scaffolds were washed three times with PBS, dehydrated with ethanol solutions (50, 60, 70, 80, 90, and 100%), coated with gold, and investigated at an accelerating voltage of 20 kV by SEM (XL30; Philips, Amsterdam, Netherlands). To assess osteogenic differentiation of MSCs, ALP (Cambridge, England, United Kingdom) activity was determined at 7 and 14 days with a colorimetric assay. Briefly, the cells on the scaffolds were washed with PBS (PH 7.4), and then lysed in assay buffer by sonication. The cell lysate (100 µL) was then mixed with 100 µL of p-nitrophenyl phosphate (pNPP) substrate solution. After incubation at 37 °C and 5% CO_2 for 1 h, NaOH was added to stop the reaction, and the absorbance was measured at 405 nm using a microplate reader.

2.5 Statistical analysis

All the results have been presented as mean ± standard deviation (SD) and analyzed by one-way ANOVA with Tukey's multiple comparison test.

3 Results

3.1 Nanoparticles characterization

XRD patterns of β-TCP and β-TCP-Sr are presented in (Fig. 2). Three intense diffraction peaks were observed at $2\theta = 30°–40°$ for β-TCP and β-TCP-Sr samples. For β-TCP-Sr composition, CaP, Sr and SrO phases were also detected (ICDD ref, codes 00-009-0169, 01-089-4047, 00-001-0886 with 60, 10 and 7% phase percent, respectively). The presence of CaP phase (ICDD ref, code 00-009-0169 with 73% phase percent) and a less intense peak of calcium pyrophosphate ($Ca_2P_2O_7$) and hydroxyapatite (HAp) (ICDD ref, code 00-011-0177 and 01-072-1243 with 19% and 9% phase percent respectively) indicated the calcium phosphate-ceramic structure of the β-TCP. While no α-TCP peaks were detected in the spectra, a slight peak shift for β-TCP-Sr specimens was detectable. A Shift in 2θ for Sr-doped β-TCP confirmed substitution of Ca^{2+} with Sr^{2+} in β-TCP network. Such peak shifts as the result of dopant addition, are common and have been extensively described elsewhere [43–45]. FT-IR spectra of β-TCP and β-TCP-Sr samples are shown in Fig. 2. β-TCP sample had two bands at 551 and 605 cm^{-1} that were due to O–P–O bending mode. The bands at 1020 and 1090 cm^{-1} were assigned to asymmetric stretching mode, and 968 cm^{-1} band was correlated with symmetric stretching vibration. From the FT-IR of β-TCP-Sr, some band shifts were observed, and two new bands at 1424.03 and 2819.51 cm^{-1} appeared, representing the presence of SrO [33]. The energy dispersive x-ray spectroscopy (EDAX) confirmed the presence of calcium, phosphorus and oxygen (Fig. 3A) and strontium (Fig. 3B) elements, in β-TCP and SrO samples. The presence of Au in β-TCP and β-TCP-Sr nanoparticles may be due to the gold coating. Figure 3C, D depict the hydrodynamic diameter of β-TCP and β-TCP-Sr nanoparticles. DLS shows a narrow hydrodynamic diameter profile of nanoparticles between 70 and 140 nm with peaks around 109 nm (Fig. 3C) and 85.1 nm (Fig. 3D) for β-TCP and β-TCP-Sr nanoparticles, respectively. The polydispersity index (PDI) for β-TCP and β-TCP-Sr nanoparticles, were 0.175 and 0.270, respectively.

3.2 Scaffold characterization

FT-IR spectra (Fig. 4A) for COL scaffold showed C=O stretch coupled with COO–- at 1665 cm^{-1} for amide I, N–H bending coupled with CN stretching at 1551 cm^{-1} for amide II, N–H bending coupled with CN stretching at 1237 cm^{-1} for amide III band, N–H stretch coupled with hydrogen bond at 3332 cm^{-1} for amide A, and C–H asymmetrical stretch at 2942 for amide B. Amide I band is generally considered as a sensitive indicator of the secondary structure. By β-TCP and β-TCP-Sr addition, frequency of the band determined for amide I region remained unchanged at 1600-1700 cm^{-1}, suggesting that the secondary structure of collagen scaffolds remained stable in COL, COL/β-TCP and COL/β-TCP-Sr. Moreover, the shifted amide A from 3320 cm^{-1} in COL/β-TCP to

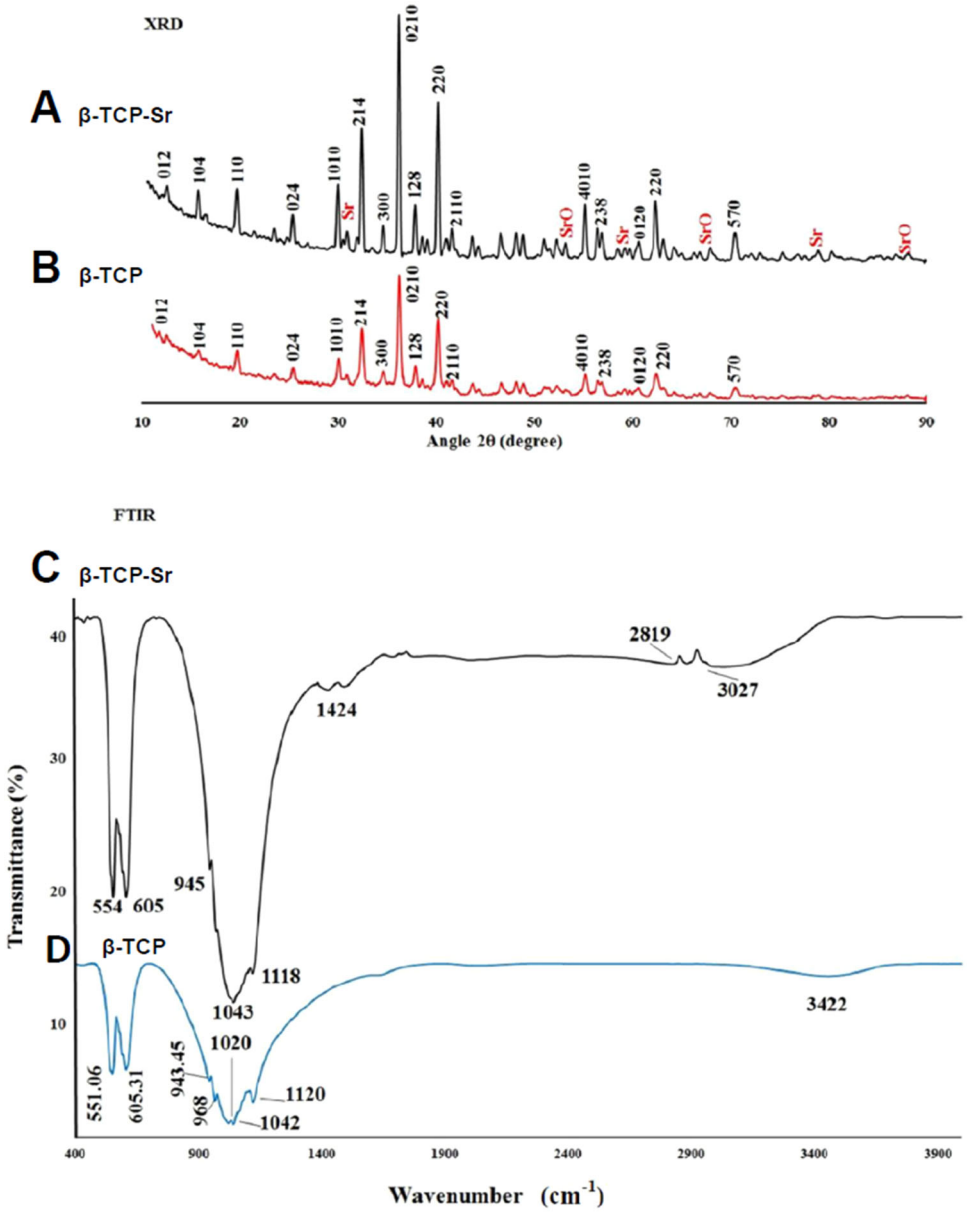

Fig. 2 **A**, **B** X-ray diffraction (XRD) patterns of β-TCP-Sr and β-TCP to detect calcium phosphate and strontium oxide phases. **C** FT-IR spectrum of β-TCP-Sr sample in which new bands related to the presence of SrO in β-TCP were observed. **D** FT-IR spectrum of β-TCP shows bending mode, asymmetric stretching mode, and symmetric stretching vibration

3314 cm^{-1} in COL/β-TCP-Sr may be due to the addition of strontium oxide [46]. Figure 4B shows SEM image of the scaffolds. All scaffolds had porous and interconnected structures, which is of particular importance for cell proliferation and migration in bone tissue engineering applications. As shown (Fig. 4B), β-TCP and β-TCP-Sr nanoparticles have been homogenously distributed in the collagen phase. Furthermore, average pore sizes of the scaffolds were investigated by image J analysis [47]. COL scaffold had an average pore diameter of 184 ± 6 μm, while COL/β-TCP and COL/β-TCP-Sr showed an average diameter of 156 ± 10 and 153 ± 9 μm, respectively. All scaffold types had porous networks with pore sizes ranging from 100 to 200 μm, which is thought to be suitable for bone tissue growth and cell attachment. Porosity of the collagen scaffold calculated from Eq. (3), was 99.1% ± 1.67, while it was 98.3% ± 1.85 and 97.6% ± 2.11 for COL/β-TCP and COL/β-TCP-Sr, respectively.

The measured compressive modulus of COL, COL/β-TCP, and COL/β-TCP-Sr were 27.94 ± 0.17, 33.14 ± 1.77 and 213.44 ± 0.47 kPa, respectively. There was no statistically significant difference ($p > 0.05$) between COL and COL/β-TCP scaffolds, demonstrating that the compressive modulus was not affected by the addition of β-TCP. Nevertheless, doping Sr with β-TCP significantly increased the mechanical strength compared with that of the other groups with no Sr ($p < 0.05$).

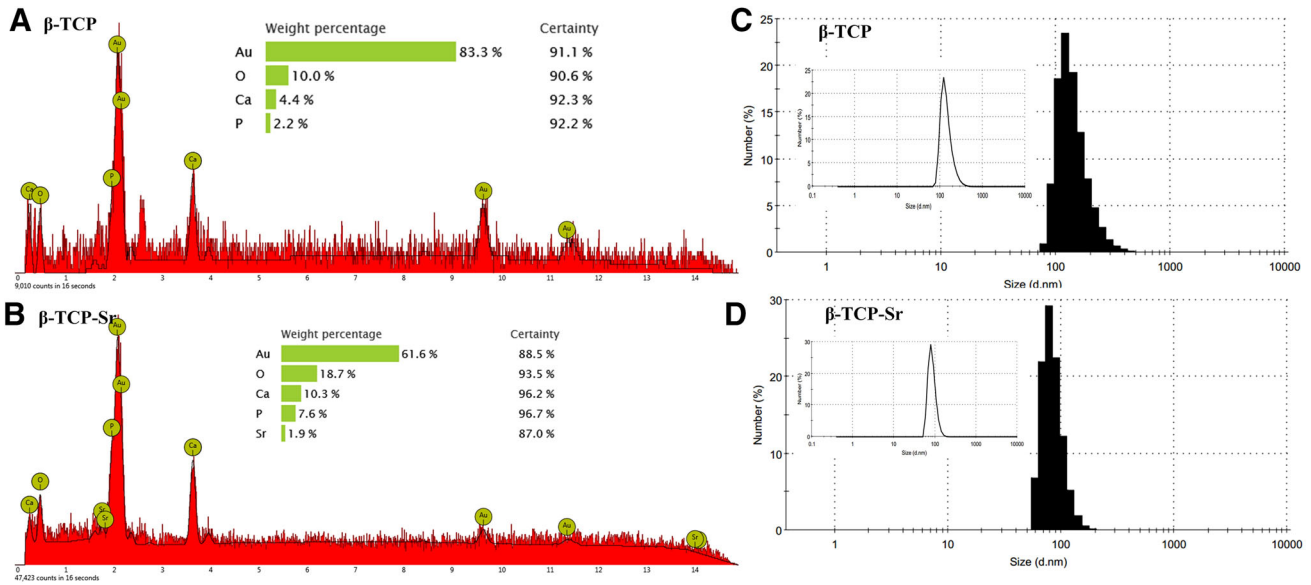

Fig. 3 EDAX spectrum of β-TCP and β-TCP-Sr nanoparticles. **A**, **B** The presence of calcium, phosphorus and oxygen and strontium elements, in β-TCP and SrO samples were confirmed. The presence of Au in β-TCP and β-TCP-Sr nanoparticles is due to the gold coating. **C**, **D** Particle size distribution of β-TCP and β-TCP-Sr from DLS investigations. The DLS curves show sharp peaks about ∼ 109 and 85.1 nm for β-TCP and β-TCP-Sr nanoparticles, respectively

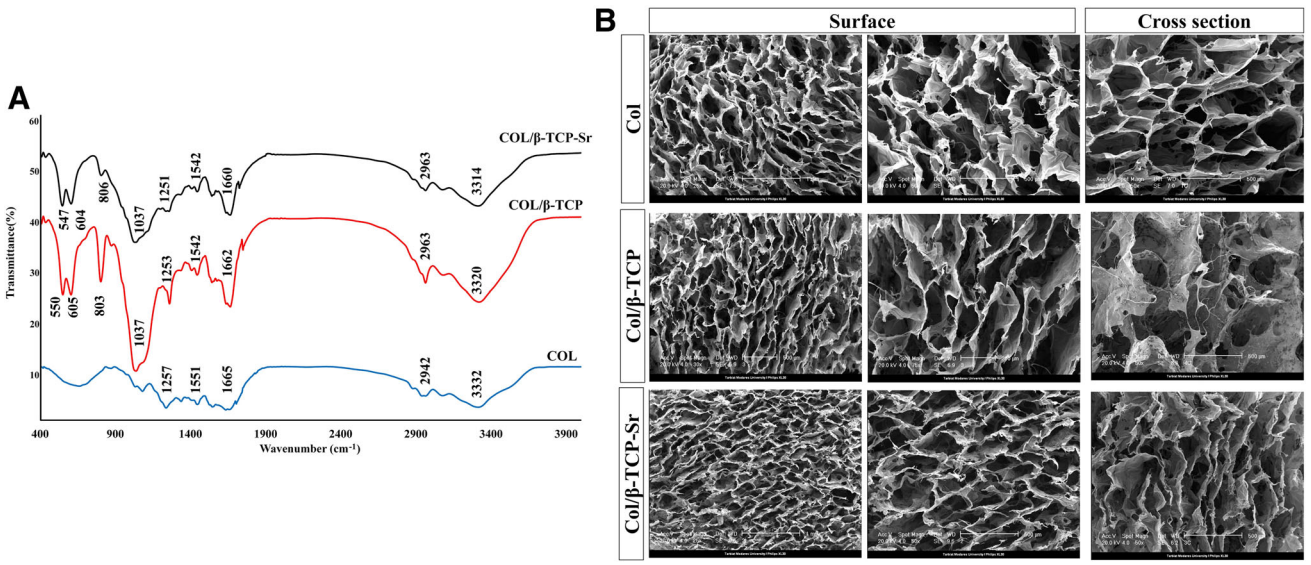

Fig. 4 FTIR was used to detect amide I, II, III, A, B and phosphate bands. **A** FT-IR spectra of COL, COL/β-TCP and COL/β-TCP-Sr samples. **B** SEM images of the surface morphology of COL, COL/β-TCP and COL/β-TCP-Sr scaffolds. All the scaffolds had porous and interconnected structures

Swelling behavior of the scaffolds is shown in Fig. 5A. Collagen swelling increased to 17.61 ± 1.51 within 3 h, and continued to increase slowly until a plateau was reached at 19.16 ± 1.23. The maximum swelling of COL/β-TCP and COL/β-TCP-Sr scaffolds were approximately 8.5 ± 0.09 and 3.5 ± 0.15 after 3 h, respectively. The swelling ratio results showed that all scaffolds reached the equilibrium swelling point before 24 h. The quantitative weight loss for all scaffold types is depicted in Fig. 5B. As shown, all scaffolds showed a mass loss over 60 days, and this weight loss was faster during the first 15 days. Our findings indicate that COL scaffold lost 56% ± 2.27 of its weight after 15 days and reached 32% ± 1.89 of the initial weight during the incubation time. Notably, the degradation rate was much slower for scaffolds containing β-TCP and β-TCP-Sr, with a reduction of only approximately 30% ± 1.25 and 25% ± 1.77 over 60 days, respectively.

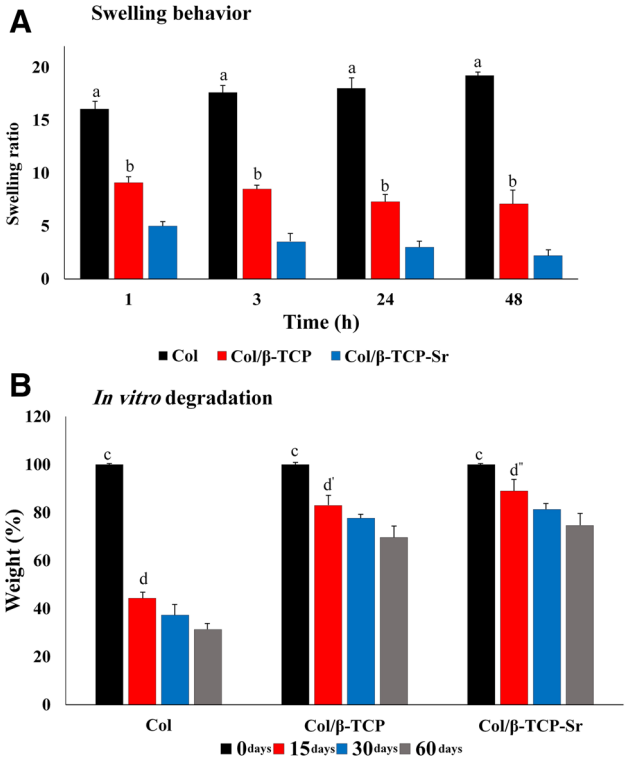

Fig. 5 **A** Swelling ratio, a: highly significant compared with other groups in all of the time points (COL/β-TCP and COL/β-TCP-Sr; $^{**}p < 0.01$), b: significant compared with COL/β-TCP-Sr group in all of the time points ($^{*}p < 0.05$). **B** *In vitro* degradation, c: highly significant in initial time points compared with other groups (COL, COL/β-TCP, and COL/β-TCP-Sr) after 60 days ($^{**}p < 0.01$), d: significant at 15 days compared with 30 days in COL group ($^{*}p < 0.05$), also highly significant at 15 days compared with 60 days in COL group, d′: significant at 15 days compared with 30 days in COL/β-TCP group ($^{*}p < 0.05$), also highly significant at 15 days compared with 60 days in COL/β-TCP group, d″: significant at 15 days compared with 30 days in COL/β-TCP-Sr group ($^{*}p < 0.05$), also highly significant at 15 days compared with 60 days in COL/β-TCP-Sr group

In vitro bioactivity of the scaffolds were characterized in standard SBF solution at physiological pH and 25 °C after 3 and 7 days. SEM analysis (Fig. 6) showed mineral deposition on the surface of COL/β-TCP and COL/β-TCP-Sr after 7 days. Moreover, EDAX spectra taken after 3 and 7 days immersion in SBF are shown in Fig. 7. Significant apatite formation was observed on the surface of COL/β-TCP-Sr sample when compared with COL/β-TCP.

SEM analysis of the surface of COL, COL/β-TCP and COL/β-TCP-Sr scaffolds seeded with rBM-MSCs after 48 h, shows cells adhesion and proliferation on the surface of all scaffolds (Fig. 8). rBM-MSCs were spread on the surface of scaffolds after 48 h of culture, and secreted ECM that indicates the satisfactory biocompatibility of scaffolds. Cell viability was assessed by MTT assay after 96 h incubation. As shown in Fig. 9, all types of scaffolds showed cellular proliferation during 96 h. No significant difference in viability was found between different groups of scaffolds after 96 h. However, the cells cultured on TCP maintained higher cell viability compared to the scaffolds ($p < 0.05$). Variations in ALP activity are shown in Fig. 10 with three replications after 7 and 14 days of culture. There are differences in ALP activity between all types of the scaffolds after 7 days of culture. ALP activity increased in all types of the scaffolds until 14 days, with a sharp increase in COL/β-TCP-Sr sample due to the presence of strontium ion in the structure. ALP activity increased 1.59-3.55 and 1.79-4.57 fold due to the presence of β-TCP and Sr^{2+} after 14 days, respectively. Notably, the addition of β-TCP-Sr to the pure collagen scaffolds increased ALP activity by 1.33-1.79 and 2.92-4.57 fold after 7 and 14 days, respectively.

4 Discussion

Previous studies have shown that incorporating of strontium into the bone scaffolds can inhibit bone resorption and stimulate new bone formation [48]. β-TCP is generally used as a bone substitute bioceramic with a high chemical similarity to the inorganic components of bone. However, the degradation profile of β-TCP is not ideal for many applications in bone tissue engineering [49]. Metal ion substitution has been shown to significantly influence the mechanical and biological properties of β-TCP [50]. Previous studies have shown that SrO incorporation into β-TCP structure enhances *in vitro* osteoblast cell attachment. β-TCP implants doped with 1.0 wt% SrO showed suitable *in vivo* biocompatibility when examined in male Sprague–Dawley rats for 16 weeks [51]. Qiu et al. [52] reported that β-TCP containing 1.0% Sr was the optimal proportion for higher osteoblastic cell growth. Another study has shown that incorporating of strontium into the β-TCP structure promotes osteoclast-like-cells resorption, and enhances cell differentiation [29]. In the present study, we hypothesized that incorporation of 1% wt Sr ions into the β-TCP network can enhance the physicochemical and biological properties of the collagen scaffold.

Chemical structure of collagen showed an abundance of carboxylic acids and amine groups (Fig. 1B). The homogeneous COL/β-TCP composite was stabilized by EDC/NHS cross-linking system. EDC/NHS provides short-range intramolecular cross-linking, which in turn improves the scaffold strength. It is assumed that short-range amide and phosphodiester bonds create scaffolds with a network structure. As shown in Fig. 1B, EDC/NHS facilitates the formation of short-range amide and phosphodiester bonds by linking a carboxylic group of collagen with an amine group on the collagen and also, a carboxylic group of collagen with a phosphate group of β-TCP [53]. The

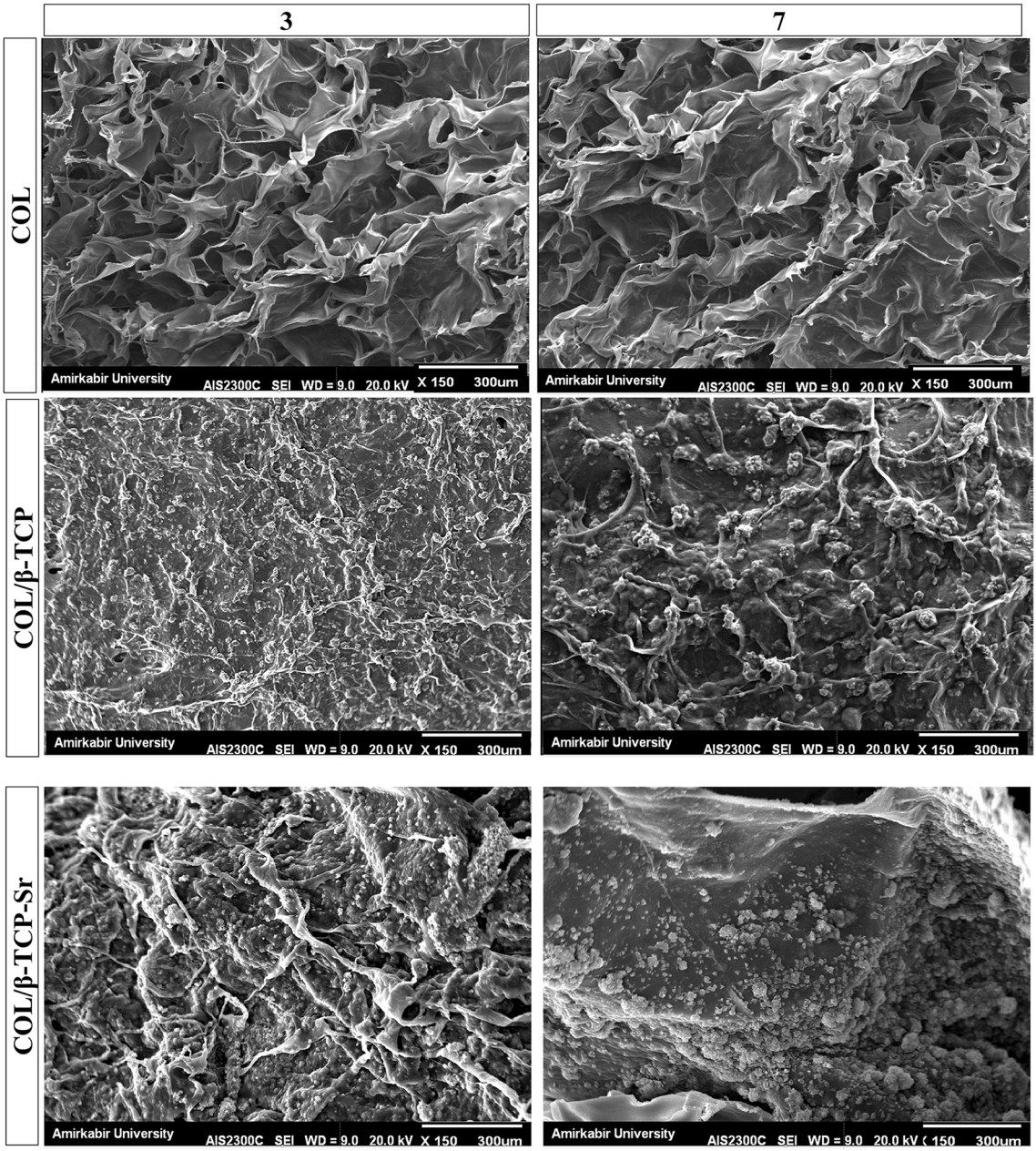

Fig. 6 SEM images show the mineralization of COL, COL/β-TCP and COL/β-TCP-Sr scaffolds in SBF, after 3 and 7 days of incubation. Collagen scaffold was selected as the control group and apatite formation was not observed on the surface of collagen scaffold

scaffold morphology is a crucial feature of the scaffolds to be used for bone tissue regeneration, and is of great importance for cell attachment and nutrient supplement. Here, an interconnected porous structure, similar to cancellous bone was generated during the freeze-drying process [22, 54]. Porosity facilitates cell migration and vascularization, and it has been reported that composites prepared by freeze-drying method have larger pore sizes. The nanocomposite scaffolds have enough porosity and proper pore size to allow for vascularization and cell proliferation. The porosity of trabecular bone is 50–95%, while more tissue ingrowth and new bone formation occur in higher porosity regions after implantation [8, 9, 55]. Thus, our findings suggested that porosity of the prepared scaffolds ($\sim$ 95–99%) was sufficient for cell adhesion and proliferation.

Providing sufficient mechanical strength is a significant criterion for tissue-engineered scaffolds. Therefore, evaluation of mechanical properties, especially compressive modulus, is crucial for the production of scaffolds for bone tissue applications [1]. Collagen- based scaffolds generally show a limited range of mechanical properties. To address

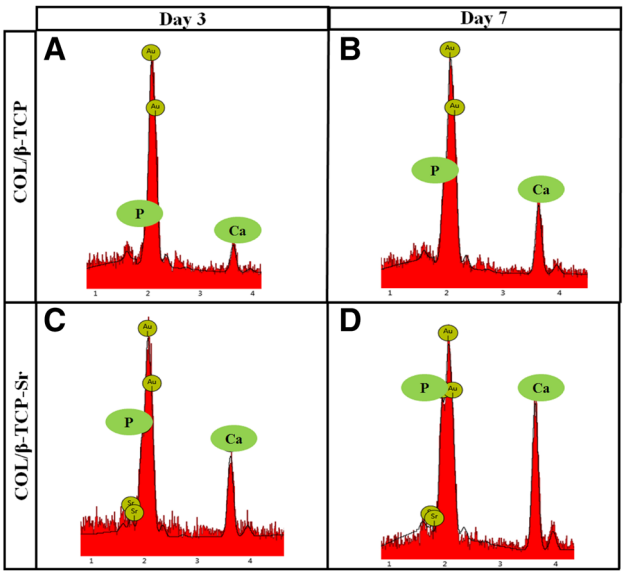

Fig. 7 EDAX analysis for COL/β-TCP and COL/β-TCP-Sr scaffolds in SBF after 3 (**A**, **C**) and 7 days (**B**, **D**). The amount of phosphorous and calcium ions was increased at the surface of COL/β-TCP-Sr scaffolds compared to COL/β-TCP, after 7 days

this problem, collagen scaffolds have been prepared with bioceramics. The improvement in the mechanical properties after addition of β-TCP-Sr particles may be influenced by some factors, including homogeneous dispersion of the particles within the polymer matrix, strong interactions between the particles and polymer, and particle size. Likewise, the improvement in mechanical properties of the scaffolds containing β-TCP-Sr nanoparticles may be due to several divalent metal ions, such as calcium and strontium, which can form ionic bonds with the carboxyl (COOH) groups on the collagen polypeptides, and therefore, influence the organization of collagen network. Our findings demonstrated that the incorporation of Sr in COL/β-TCP improved the scaffolds compressive modulus. Previously, Tarafder et al. [24] created three scaffolds (1: pure TCP: conventional sintering, 2: pure TCP: microwave sintering, and 3: Sr-Mg-Doped TCP: microwave sintering with different particle sizes (1000, 750, and 500 μm)). They found a significant difference between the groups 1 and 2, with 3 for each particle size, suggesting an increase in the compressive modulus of the scaffold as the result of Sr and Mg addition. However, this improvement depended on the particle size and its homogeneous dispersion within the polymeric matrix. Dispersion affects the interactions between the polymer and particles. Furthermore, they showed a significant improve in the compressinve modulus by decreasing the particle size. Hence, particle size positively affects the mechanical properties. Therefore, not only a small increase in divalent ions influences the mechanical properties, but also a change in the particle size has a positive impact on improving the compressive modulus [56]. Zhang et al. [57] prepared 3-D porous Sr-containing mesoporous bioactive glass (MBG) scaffolds using a 3-D printing technique. Importantly, the 3-D printed Sr-MBG scaffolds exhibited a high compressive strength of ~ 8–9 MPa, which was greater than or comparable with the MBG scaffolds. John et al. [58] prepared new organic–inorganic hybrid scaffolds [hybrid calcium phosphate (HCPP) and strontium doped HCPP (HCPSP)]. The value of compressive modulus showed that HCPSP had a higher compressive modulus (21.7 ± 2.3 GPa) compared to HCPP (21.3 ± 2.4 GPa).

Scaffold swelling plays a significant role in tissue culture, and affects cell attachment and differentiation. Swelling ratio of the nanocomposite scaffolds is associated with the bioactive ceramic content and cross-linking process [22]. Our findings showed that the swelling ratio decreased by addition the nanoparticles. This may be due to the presence of β-TCP-Sr and β-TCP, which resulted in cross-linking between the chains, and decreased the hydrophilicity of collagen by the linkage of phosphate $\left(PO_4^{3-}\right)$ and calcium (Ca^{2+}) or strontium (Sr^{2+}) to the hydrophilic NH_2 or COOH groups. The combination of calcium phosphate with strontium inhibits the extension of polymer chains, which subsequently decreases the swelling ratio. Dispersion of β-TCP and β-TCP-Sr nanoparticles in the collagen could improve the structural constancy of the nanocomposite scaffolds.

Biodegradation rate of the scaffold is an essential feature in substitution with newly formed tissue [58]. The combination of β-TCP and the polymeric scaffold changes the bulk and surface properties of the scaffold, and therefore, can affect the polymer degradation characteristics. The dissolution of alkaline ions (e.g., Ca^{2+} and Sr^{2+}) from the β-TCP-Sr structure neutralizes the possible acidic by-products of polymer degradation and prevents the autocatalytic degradation [3]. Furthermore, substitution of calcium ions with larger ions, such as strontium, leads to decreased irregularity of the network, as a result of the lower disruption rate of Sr-doped β-TCP. We confirmed the lower degradation rate of scaffolds containing Sr compared with that of the Sr-free scaffolds, and showed rapid degradation of the pure collagen scaffold over a 2-week period. Therefore, β-TCP and β-TCP-Sr nanoparticles prevented rapid degradation of nanocomposite structure. The reduced degradation rate of COL/β-TCP-Sr scaffold might be beneficial as it can provide sufficient time for the formation of ECM during tissue regeneration [8].

The apatite-formation ability of a scaffold in SBF is useful for predicting the *in vivo* bone formation [59]. The amount of phosphorous and calcium ions at the surface of

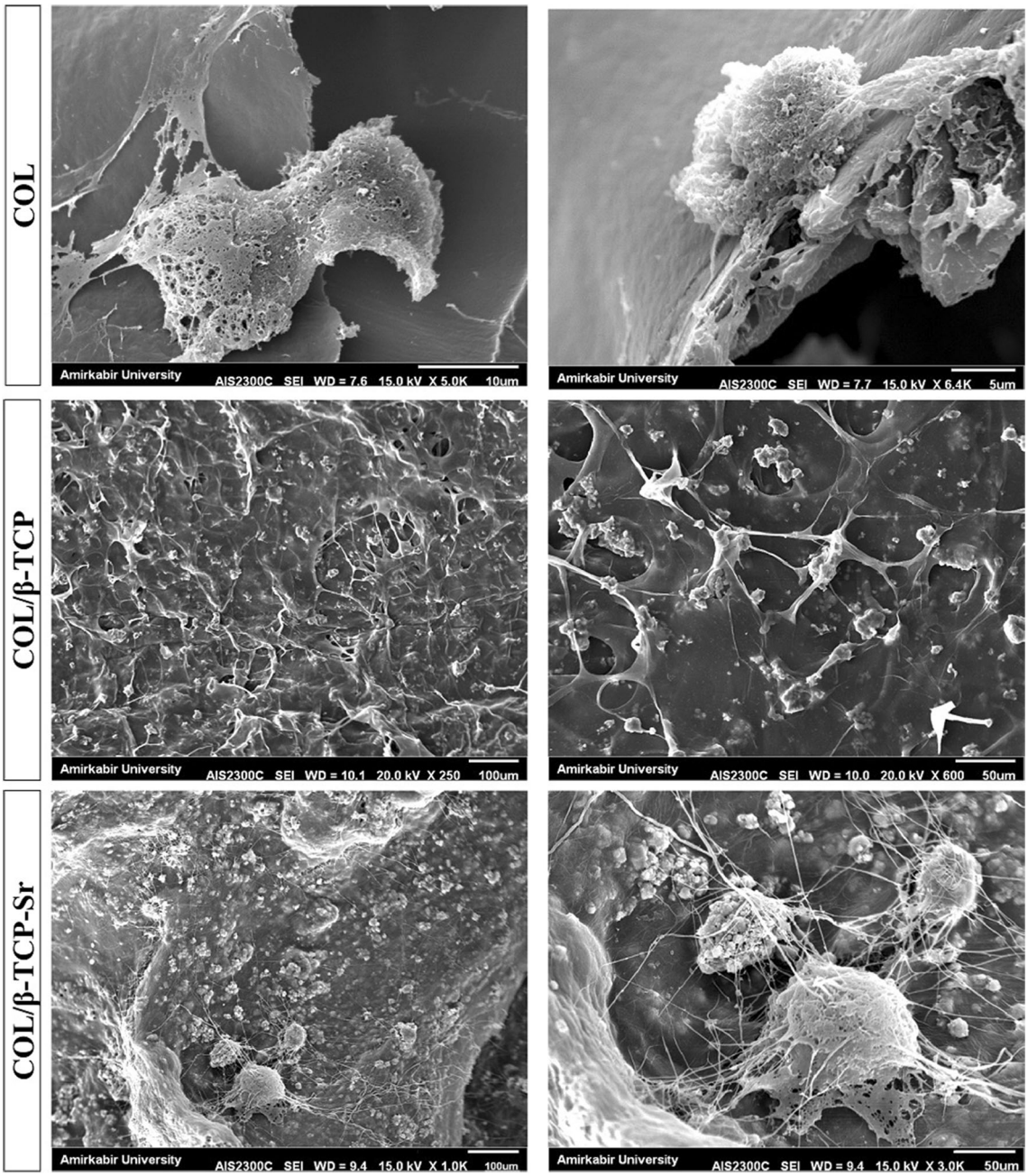

Fig. 8 SEM images of COL, COL/β-TCP and COL/β-TCP-Sr scaffolds seeded with BM-MSCs, after 48 h. COL/β-TCP-Sr scaffold showed better cell spreading compared to the other samples

COL/β-TCP-Sr scaffolds increased during the experiment, due to higher ionic radius of Sr^{2+} (113 pm) compared to Ca^{2+} (99 pm). High surface area of β-TCP-Sr induced high chemical reactivity, and thereby resulted in good bone-forming bioactivity. Thus, substitution of Ca with Sr expands the crystal structure of β-TCP, assuming that Sr creates a substitution defect, which can lead to a higher Ca^{2+} release from β-TCP–Sr [50, 57]. The scaffold containing Sr had a good apatite-forming bioactivity, and can bond well to live bone after implantation *in vivo* [57]. It was also shown that the addition of Sr enhanced mineralization of the scaffolds, which is important for cellular attachment and osteointegration [28].

Cell viability on the scaffolds was lower than that on TCP. This finding agrees with a previous study [56], which showed that the lower viability may be due to rapid degradation of scaffolds. High concentration of Sr^{2+} ions (> 1 mM) remarkably suppress the proliferation of MSCs [60]. Notably, the positive effect of Sr on proliferation of MSCs was not always observed in other studies [48, 61].

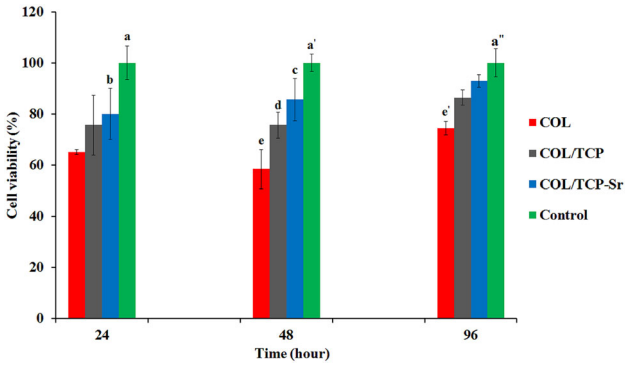

Fig. 9 Cell viability on the scaffolds, a: highly significant at 24 h in control group compared with COL and COL/β-TCP groups ($^{**}p < 0.01$) and significant compared with COL/β-TCP-Sr group ($^{*}p < 0.05$), a′: highly significant at 48 h in control group compared with COL and COL/β-TCP groups ($^{**}p < 0.01$), c: highly significant at 48 h in COL/β-TCP-Sr group compared with COL group ($^{**}p < 0.01$), a″: highly significant at 96 h in control group compared with COL group ($^{**}p < 0.01$)

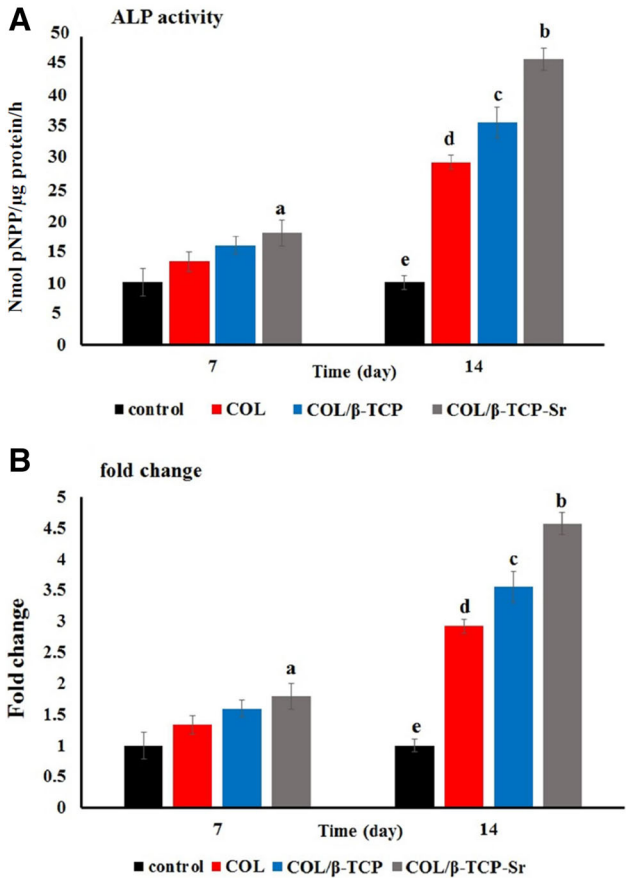

Fig. 10 **A** Comparison of ALP activity for the cells in different groups after 7 and 14 days. The cells cultured on tissue culture plate (TCP) were considered as control group. **B** Fold change of COL, COL/β-TCP and COL/β-TCP-Sr scaffolds at each time point, a: significant at 7 days in COL/β-TCP-Sr group compared with other group ($^{*}p < 0.05$), b: highly significant at 14 days in COL/β-TCP-Sr group compared with control (e) and COL (d) groups ($^{**}p < 0.01$) and significant compared with COL/β-TCP group ($^{*}p < 0.05$), c: highly significant at 14 days in COL/β-TCP group compared with control ($^{**}p < 0.01$) and significant compared with COL group ($^{*}p < 0.05$), d: highly significant at 14 days in COL group compared with control ($^{**}p < 0.01$)

For instance, Cheng et al. [48] reported that MSCs showed a similar proliferation rate when comparing calcined porcine bone/polycaprolaptone/Sr (CPB/PCL/Sr) and CPB/PCL scaffolds. Here, Sr content was about 1.02% in β-TCP structure, as it has been reported that 1.0% Sr in calcium phosphate ceramics is required for optimal cell growth [32, 52, 62, 63]. COL/β-TCP-Sr scaffold (Fig. 8) provided better cell spreading compared to the other samples, implying that Sr enhanced rBM-MSCs attachment and proliferation on the scaffolds. In addition, the incorporation of Sr in β-TCP plays an important role in the adhesion, spreading and morphology of rBMSCs, but had little effect on the proliferation. These findings suggest that β-TCP and Sr incorporated collagen scaffolds provided a favorable environment for adhesion of MSCs [22, 29].

Differentiation of rBM-MSCs is one of the key factors for bone tissue engineering. Differentiation of rBM-MSCs into osteoblast phenotype was determined using ALP activity [2]. The results of ALP activity indicated that β-TCP-Sr could effectively promote osteoblast differentiation compared with β-TCP, which may be duo to the presence of Sr in the nanocomposite scaffold [31, 64]. Moreover, the presence of Ca^{2+} can enhance osteoblast differentiation, and higher Ca concentration on COL/β-TCP-Sr surface (as shown in Fig. 9) also contributed to this effect. Qiu et al. [52, 65] showed that Sr-doped CaP scaffolds could stimulate the differentiation of osteoblastic ROS17/2.8 cells. In another study, Zreiqat et al. showed that incorporation of Sr into a calcium silicate ceramic had a stimulatory effect on the differentiation of osteoblast cells. The exact mechanism of Sr^{2+} effect on the bone cells remains unknown, although it has been proposed that Sr acts on the calcium sensing receptor (CaSR) expressed by bone cells, and thus interacts with signaling pathways. Furthermore, an increase in β-catenin expression indicates an enhanced transcription of osteogenic factors, which in turn inhibits the formation of osteoclasts and their resorption activity [28]. The presence of Sr^{2+} in the doped TCP was beneficial for osteogenic differentiation of MSCs present in the bone marrow.

In this study, a new nanocomposite scaffold has been successfully developed by freeze-drying method, using a combination of collagen, β-TCP and SrO. COL/β-TCP-Sr nanocomposite scaffold was prepared for bone tissue applications and compared to COL/β-TCP scaffolds to clarify the effect of metallic ion (Sr^{2+}) on the physico-chemical and biological properties. The scaffolds containing Sr exhibited higher mechanical strength, slower degradation rate, lower swelling ratio and higher

differentiation ability compared with those without Sr. It was also shown that incorporation of Sr into the structure of collagen-β-TCP scaffold has a great potential for bone tissue engineering applications.

Acknowledgement We thank Tarbiat Modares University for supporting this work.

Compliance with ethical standards

Conflict of interest The authors declare that they have no conflict of interest.

Ethical statement Animal experiments were approved by the Ethics Committee of Tarbiat Modares University, Iran (IR.TMU.REC.1395.412).

References

1. Arahira T, Todo M. Variation of mechanical behavior of β-TCP/collagen two phase composite scaffold with mesenchymal stem cell in vitro. J Mech Behav Biomed Mater. 2016;61:464–74.
2. Aghajanpoor M, Hashemi-Najafabadi S, Baghaban-Eslaminejad M, Bagheri F, Mohammad Mousavi S, Azam Sayyahpour F. The effect of increasing the pore size of nanofibrous scaffolds on the osteogenic cell culture using a combination of sacrificial agent electrospinning and ultrasonication. J Biomed Mater Res A. 2017;105:1887–99.
3. Baheiraei N, Azami M. Investigation of fluorine incorporation within gelatin/calcium phosphate nanocomposite scaffold prepared through a diffusion method. Adv Compos Lett. 2013;22:106–12.
4. Baheiraei N, Azami M, Hosseinkhani H. Investigation of magnesium incorporation within gelatin/calcium phosphate nanocomposite scaffold for bone tissue engineering. Int J Appl Ceram Technol. 2015;12:245–53.
5. Azami M, Tavakol S, Samadikuchaksaraei A, Hashjin MS, Baheiraei N, Kamali M, et al. A porous hydroxyapatite/gelatin nanocomposite scaffold for bone tissue repair : in vitro and in vivo evaluation. J Biomater Sci Polym Ed. 2012;23:2353–68.
6. Matsuno T, Nakamura T, Kuremoto K, Notazawa S, Nakahara T, Hashimoto Y, et al. Development of beta-tricalcium phosphate/collagen sponge composite for bone regeneration. Dent Mater J. 2006;25:138–44.
7. Hong S, Kim M, Kim G. Collagen–β-TCP conjugated PCL biocomposites for bone tissue regeneration: fabrication, physical properties, and cellular activities. J Mater Chem. 2012;22:22565–74.
8. Shavandi A, Bekhit Ael-D, Bekhit A, Sun Z, Ali A, Gould M. A novel squid pen chitosan/hydroxyapatite/beta-tricalcium phosphate composite for bone tissue engineering. Mater Sci Eng C Mater Biol Appl. 2015;55:373–83.
9. Muthukumar T, Aravinthan A, Sharmila J, Kim NS, Kim JH. Collagen/chitosan porous bone tissue engineering composite scaffold incorporated with Ginseng compound K. Carbohydr Polym. 2016;152:566–74.
10. Zhang ML, Cheng J, Xiao YC, Yin RF, Feng X. Raloxifene microsphere-embedded collagen/chitosan/β-tricalcium phosphate scaffold for effective bone tissue engineering. Int J Pharm. 2017;518:80–5.
11. Patntirapong S, Janvikul W, Theerathanagorn T, Singhatanadgit W. Osteoinduction of stem cells by collagen peptide-immobilized hydrolyzed poly(butylene succinate)/β-tricalcium phosphate scaffold for bone tissue engineering. J Biomater Appl. 2017;31:859–70.
12. Baheiraei N, Nourani MR, Mortazavi SMJ, Movahedin M, Eyni H, Bagheri F, Norahan MH. Development of a bioactive porous collagen/β-tricalcium phosphate bone graft assisting rapid vascularization for bone tissue engineering applications. J Biomed Mater Res A. 2018;106:73–85.
13. Wagner DE, Eisenmann KM, Nestor-Kalinoski AL, Bhaduri SB. A microwave-assisted solution combustion synthesis to produce europium-doped calcium phosphate nanowhiskers for bioimaging applications. Acta Biomater. 2013;9:8422–32.
14. Wagner DE, Jones AD, Zhou H, Bhaduri SB. Cytocompatibility evaluation of microwave sintered biphasic calcium phosphate scaffolds synthesized using pH control. Mater Sci Eng C Mater Biol Appl. 2013;33:1710–9.
15. Zhou Y, Xu L, Zhang X, Zhao Y, Wei S, Zhai M. Radiation synthesis of gelatin/CM-chitosan/β-tricalcium phosphate composite scaffold for bone tissue engineering. Mater Sci Eng C Mater Biol Appl. 2012;32:994–1000.
16. Zhu Q, Ablikim Z, Chen T, Cai Q, Xia J, Jiang D, et al. The preparation and characterization of HA/β-TCP biphasic ceramics from fish bones. Ceram Int. 2017;43:12213–20.
17. Das S, Jhingran R, Bains VK, Madan R, Srivastava R, Rizvi I. Socket preservation by beta-tri-calcium phosphate with collagen compared to platelet-rich fibrin: A clinico-radiographic study. Eur J Dent. 2016;10:264–76.
18. Choi MO, Kim YJ. Fabrication of gelatin/calcium phosphate composite nanofibrous membranes by biomimetic mineralization. Int J Biol Macromol. 2012;50:1188–94.
19. Kim W, Jang CH, Kim G. Optimally designed collagen/polycaprolactone biocomposites supplemented with controlled release of HA/TCP/rhBMP-2 and HA/TCP/PRP for hard tissue regeneration. Mater Sci Eng C Mater Biol Appl. 2017;78:763–72.
20. Serra IR, Fradique R, Vallejo MC, Correia TR, Miguel SP, Correia IJ. Production and characterization of chitosan/gelatin/β-TCP scaffolds for improved bone tissue regeneration. Mater Sci Eng C Mater Biol Appl. 2015;55:592–604.
21. Best SM, Porter AE, Thian ES, Huang J. Bioceramics: past, present and for the future. J Eur Ceram Soc. 2008;28:1319–27.
22. Baheiraei N, Nourani MR, Mortazavi SMJ, Movahedin M, Eyni H, Bagheri F, et al. Development of a bioactive porous collagen/β-tricalcium phosphate bone graft assisting rapid vascularization for bone tissue engineering applications. J Biomed Mater Res A. 2018;106:73–85.
23. Cruz R, Calasans-Maia J, Sartoretto S, Moraschini V, Rossi AM, Louro RS, et al. Does the incorporation of zinc into calcium phosphate improve bone repair? A systematic review. Ceram Int. 2018;44:1240–9.
24. Tarafder S, Davies NM, Bandyopadhyay A, Bose S. 3D printed tricalcium phosphate bone tissue engineering scaffolds: effect of SrO and MgO doping on in vivo osteogenesis in a rat distal femoral defect model. Biomater Sci. 2013;1:1250–9.
25. Rentsch B, Bernhardt A, Henß A, Ray S, Rentsch C, Schamel M, et al. Trivalent chromium incorporated in a crystalline calcium phosphate matrix accelerates materials degradation and bone formation in vivo. Acta Biomater. 2018;69:332–41.
26. Lode A, Heiss C, Knapp G, Thomas J, Nies B, Gelinsky M, et al. Strontium-modified premixed calcium phosphate cements for the therapy of osteoporotic bone defects. Acta Biomater. 2018;65:475–85.
27. Bose S, Fielding G, Tarafder S, Bandyopadhyay A. Understanding of dopant-induced osteogenesis and angiogenesis in calcium phosphate ceramics. Trends Biotechnol. 2013;31:594–605.

28. Schumacher M, Gelinsky M. Strontium modified calcium phosphate cements—approaches towards targeted stimulation of bone turnover. J Mater Chem B. 2015;3:4626–40.
29. Roy M, Fielding G, Bandyopadhyay A, Bose S. Effects of zinc and strontium substitution in tricalcium phosphate on osteoclast differentiation and resorption. Biomater Sci. 2013;1:74–82.
30. Khan PK, Mahato A, Kundu B, Nandi SK, Mukherjee P, Datta S, et al. Influence of single and binary doping of strontium and lithium on in vivo biological properties of bioactive glass scaffolds. Sci Rep. 2016;6:32964.
31. Bellucci D, Sola A, Cacciotti I, Bartoli C, Gazzarri M, Bianco A, et al. Mg- and/or Sr-doped tricalcium phosphate/bioactive glass composites : Synthesis, microstructure and biological responsiveness. Mater Sci Eng C Mater Biol Appl. 2014;42:312–24.
32. Hulsart-Billström G, Xia W, Pankotai E, Weszl M, Carlsson E, Forster-Horváth C, et al. Osteogenic potential of Sr-doped calcium phosphate hollow spheres in vitro and in vivo. J Biomed Mater Res A. 2013;101:2322–31.
33. Banerjee SS, Tarafder S, Davies NM, Bandyopadhyay A, Bose S. Understanding the influence of MgO and SrO binary doping on the mechanical and biological properties of β-TCP ceramics. Acta Biomater. 2010;6:4167–74.
34. Carmo ABXD, Sartoretto SC, Alves ATNN, Granjeiro JM, Miguel FB, Calasans-Maia J, et al. Alveolar bone repair with strontium-containing nanostructured carbonated hydroxyapatite. J Appl Oral Sci. 2018;26:e20170084.
35. Liu J, Rawlinson SC, Hill RG, Fortune F. Strontium-substituted bioactive glasses in vitro osteogenic and antibacterial effects. Dent Mater. 2016;32:412–22.
36. Chen YW, Shi GQ, Ding YL, Yu XX, Zhang XH, Zhao CS, et al. In vitro study on the influence of strontium-doped calcium polyphosphate on the angiogenesis-related behaviors of HUVECs. J Mater Sci Mater Med. 2008;19:2655–62.
37. Gu Z, Xie H, Li L, Zhang X, Liu F, Yu X. Application of strontium-doped calcium polyphosphate scaffold on angiogenesis for bone tissue engineering. J Mater Sci Mater Med. 2013;24:1251–60.
38. Liu F, Zhang X, Yu X, Xu Y, Feng T, Ren D. In vitro study in stimulating the secretion of angiogenic growth factors of strontium-doped calcium polyphosphate for bone tissue engineering. J Mater Sci Mater Med. 2011;22:683–92.
39. Huang S, Xu L, Sun Y, Wu T, Wang K, Li G. An improved protocol for isolation and culture of mesenchymal stem cells from mouse bone marrow. J Orthop Translat. 2014;3:26–33.
40. Eslaminejad MB, Bagheri F, Zandi M, Nejati E, Zomorodian E, Mivehchi H. Comparison of proliferation and osteoblast differentiation of marrow-derived mesenchymal stem cells on nano- and micro-hydroxyapatite contained composite scaffolds. Iran J Biotechnol. 2010;8:234–42.
41. Mohtashamian S, Boddohi S, Hosseinkhani S. Preparation and optimization of self-assembled chondroitin sulfate-nisin nanogel based on quality by design concept. Int J Biol Macromol. 2018;107:2730–9.
42. Kavya KC, Jayakumar R, Nair S, Chennazhi KP. Fabrication and characterization of chitosan/gelatin/nSiO_2 composite scaffold for bone tissue engineering. Int J Biol Macromol. 2013;59:255–63.
43. Meenambal R, Poojar P, Geethanath S, Sanjeevi K. Structural insights in Dy^{3+}-doped b-Tricalcium phosphate and its multimodal imaging characteristics. J Am Ceram Soc. 2017;100:1831–41.
44. Nandha Kumar P, Mishra SK, Kannan S. Structural elucidation and iron oxidation states in situ formed β-$Ca_3(PO_4)_2$/α-Fe_2O_3 composites. J Am Ceram Soc. 2017;100:3746–56.
45. Stipniece L, Narkevica I, Salma-Ancane K. Low-temperature synthesis of nanocrystalline hydroxyapatite: effect of Mg and Sr content. J Am Ceram Soc. 2017;100:1697–706.
46. Feng W, Feng S, Tang K, He X, Jing A, Liang G. A novel composite of collagen-hydroxyapatite/kappa-carrageenan. J Alloys Compd. 2017;693:482–9.
47. Barabadi Z, Azami M, Sharifi E, Karimi R, Lotfibakhshaiesh N, Roozafzoon R, et al. Fabrication of hydrogel based nanocomposite scaffold containing bioactive glass nanoparticles for myocardial tissue engineering. Mater Sci Eng C Mater Biol Appl. 2016;69:1137–46.
48. Cheng D, Liang Q, Li Y, Fan J, Wang G, Pan H, et al. Strontium incorporation improves the bone-forming ability of scaffolds derived from porcine bone. Colloids Surf B Biointerfaces. 2018;162:279–87.
49. Özarslan AC, Yücel S. Fabrication and characterization of strontium incorporated 3-D bioactive glass scaffolds for bone tissue from biosilica. Mater Sci Eng C Mater Biol Appl. 2016;68:350–7.
50. Bandyopadhyay A, Petersen J, Fielding G, Banerjee S, Bose S. ZnO, SiO_2, and SrO doping in resorbable tricalcium phosphates: influence on strength degradation, mechanical properties, and in vitro bone-cell material interactions. J Biomed Mater Res B Appl Biomater. 2012;100:2203–12.
51. Banerjee SS, Tarafder S, Davies NM, Bandyopadhyay A, Bose S. Understanding the influence of MgO and SrO binary doping on the mechanical and biological properties of β-TCP ceramics. Acta Biomater. 2010;6:4167–74.
52. Qiu K, Zhao XJ, Wan CX, Zhao CS, Chen YW. Effect of strontium ions on the growth of ROS17/2.8 cells on porous calcium polyphosphate scaffolds. Biomaterials. 2006;27:1277–86.
53. Rafat M, Li F, Fagerholm P, Lagali NS, Watsky MA, Munger R, et al. PEG-stabilized carbodiimide crosslinked collagen-chitosan hydrogels for corneal tissue engineering. Biomaterials. 2008;29:3960–72.
54. Sharifi E, Azami M, Kajbafzadeh AM, Moztarzadeh F, Faridi-Majidi R, Shamousi A, et al. Preparation of a biomimetic composite scaffold from gelatin/collagen and bioactive glass fibers for bone tissue engineering. Mater Sci Eng C Mater Biol Appl. 2016;59:533–41.
55. Islam SM, Todo M. Effects of sintering temperature on the compressive mechanical properties of collagen/hydroxyapatite composite scaffolds for bone tissue engineering. Mater Lett. 2016;173:231–4.
56. Zare S, Baheiraei N, Bagheri F. The effects of strontium incorporation on a novel gelatin/bioactive glass bone graft : In vitro and in vivo characterization. Ceram Int. 2018;44:14217–27.
57. Zhang J, Zhao S, Zhu Y, Huang Y, Zhu M, Tao C, et al. Three-dimensional printing of strontium-containing mesoporous bioactive glass scaffolds for bone regeneration. Acta Biomater. 2014;10:2269–81.
58. John Ł, Podgórska M, Nedelec JM, Cwynar-Zajac Ł, Dzięgiel P. Strontium-doped organic-inorganic hybrids towards three-dimensional scaffolds for osteogenic cells. Mater Sci Eng C Mater Biol Appl. 2016;68:117–27.
59. Zhao S, Zhang J, Zhu M, Zhang Y, Liu Z, Tao C, et al. Three-dimensional printed strontium-containing mesoporous bioactive glass scaffolds for repairing rat critical-sized calvarial defects. Acta Biomater. 2015;12:270–80.
60. Lei Y, Xu Z, Ke Q, Yin W, Chen Y, Zhang C, et al. Strontium hydroxyapatite/chitosan nanohybrid scaffolds with enhanced osteoinductivity for bone tissue engineering. Mater Sci Eng C Mater Biol Appl. 2017;72:134–42.
61. Ni GX, Lu WW, Chiu KY, Li ZY, Fong DY, Luk KD. Strontium-containing hydroxyapatite (Sr-HA) bioactive cement for primary hip replacement: an in vivo study. J Biomed Mater Res B Appl Biomater. 2006;77:409–15.
62. Rohnke M, Pfitzenreuter S, Mogwitz B, Henß A, Thomas J, Bieberstein D, et al. Strontium release from Sr^{2+} -loaded bone

cements and dispersion in healthy and osteoporotic rat bone. J Control Release. 2017;262:159–69.
63. Quade M, Schumacher M, Bernhardt A, Lode A, Kampschulte M, Voß A, et al. Strontium-modification of porous scaffolds from mineralized collagen for potential use in bone defect therapy. Mater Sci Eng C Mater Biol Appl. 2017;84:159–67.
64. Li J, Dou Y, Yang J, Yin Y, Zhang H, Yao F, et al. Surface characterization and biocompatibility of micro- and nano-hydroxyapatite/chitosan-gelatin network films. Mater Sci Eng C Mater Biol Appl. 2009;29:1207–15.
65. Zreiqat H, Ramaswamy Y, Wu C, Paschalidis A, Lu Z, James B, et al. The incorporation of strontium and zinc into a calcium-silicon ceramic for bone tissue engineering. Biomaterials. 2010;31:3175–84.